Electronic Supplementary Information (ESI)

Understanding the preparative chemistry of atomically dispersed nickel catalysts for achieving high-efficiency H$_2$O$_2$ electrosynthesis

June Sung Lim,[a] Jinwoo Woo,[b] Geunsu Bae,[c] Suhwan Yoo,[a] Jinjong Kim,[a] Jae Hyung Kim,[d] Jong Hoon Lee,[e] Young Jin Sa,[f] Ji-Wook Jang,[g] Yun Jeong Hwang,[a] Chang Hyuck Choi,*[c,h] and Sang Hoon Joo*[a]

[a]*Department of Chemistry, Seoul National University, Seoul 08826, Republic of Korea.*

[b]*Lotte Chemical Institute of Technology (LCIT), Daejeon 34110, Republic of Korea.*

[c]*Department of Chemistry, Pohang University of Science and Technology (POSTECH), Pohang 37673, Republic of Korea.*

[d]*Clean Fuel Research Laboratory, Korea Institute of Energy Research (KIER), Daejeon, 34129, Republic of Korea.*

[e]*UNIST Central Research Facilities, Ulsan National Institute of Science and Technology (UNIST), Ulsan 44919, Republic of Korea.*

[f]*Department of Chemistry, Kwangwoon University, Seoul 01897, Republic of Korea.*

[g]*School of Energy and Chemical Engineering, Ulsan National Institute of Science and Technology (UNIST), Ulsan 44919, Republic of Korea.*

[h]*Institute for Convergence Research and Education in Advanced Technology (I-CREATE), Yonsei University, Seoul 03722, Republic of Korea.*

Corresponding Author

*E-mail: chchoi@postech.ac.kr (C.H.C.), shjoo1@snu.ac.kr (S.H.J.)

Table of contents

1. Supplementary figures and tables

(a)

(b)

(c)

(d)

Fig. S1 (a) Small-angle XRD pattern, (b) N_2 adsorption-desorption isotherm, (c) BJH pore size distribution curve obtained from the adsorption branch of the corresponding isotherm, and (d) BF-STEM image of SBA-15.

(a) Ni–N/C_3_Dry

(b) Ni–N/C_3_Acetone

(c) Ni–N/C_3_EtOH

(d) Ni–N/C_3_H$_2$O

100 nm
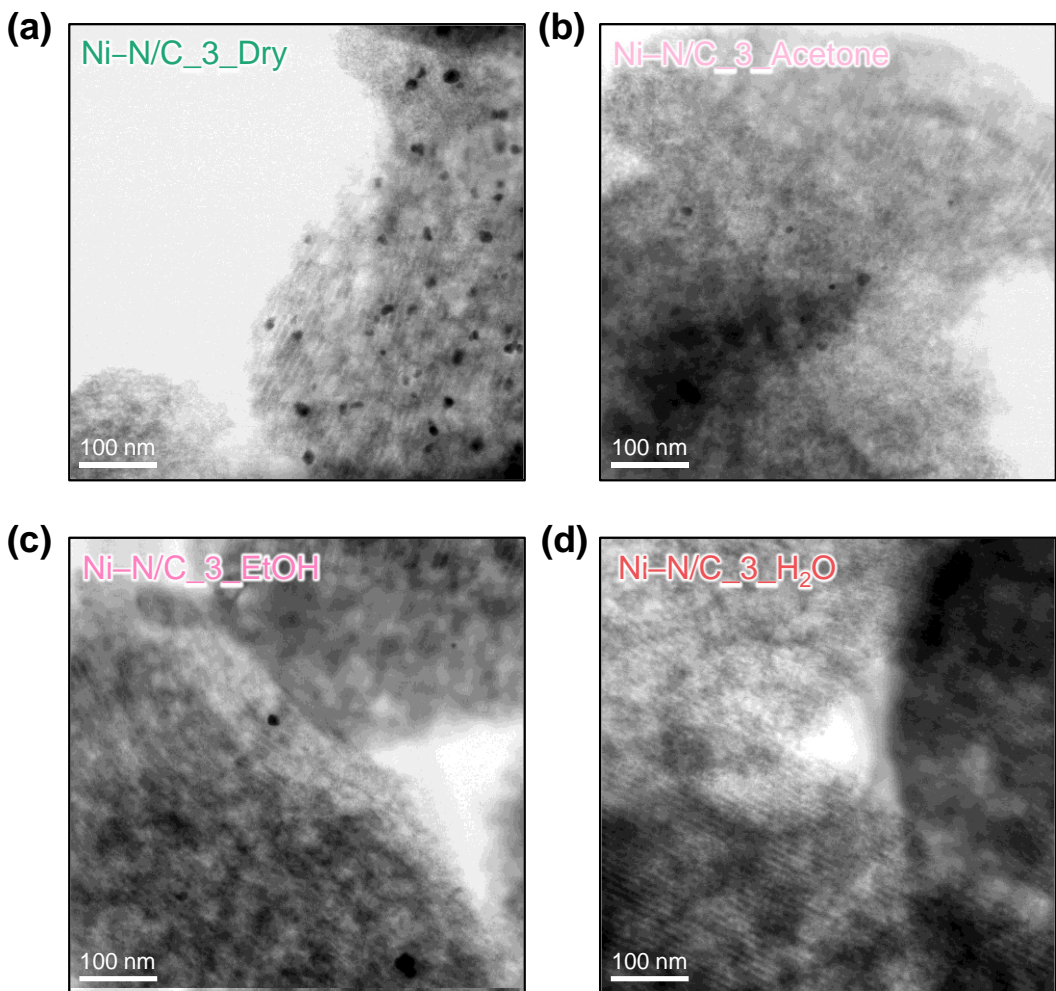
Fig. S2 BR-STEM images of (a) Ni–N/C_3_Dry, (b) Ni–N/C_3_Acetone, (c) Ni–N/C_3_EtOH, and (d) Ni–N/C_3_H$_2$O catalysts.
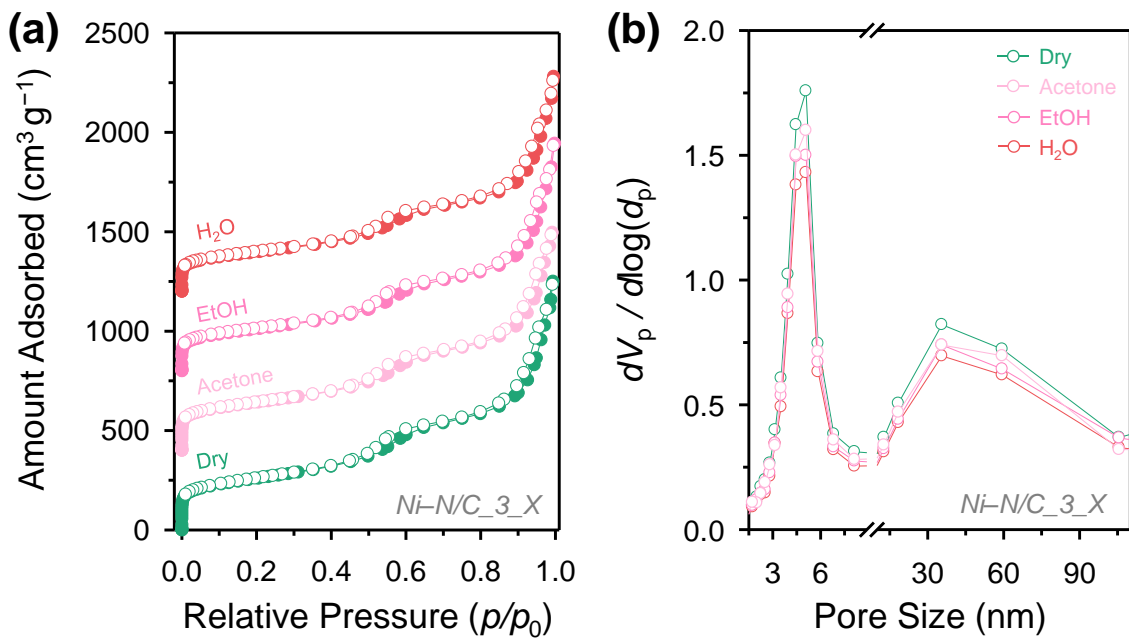
Fig. S3 (a) N_2 adsorption-desorption isotherms and (b) BJH pore size distribution curves obtained from the adsorption branch of the corresponding isotherms of Ni–N/C_3_*X* catalysts. The isotherms of Ni–N/C_3_Acetone, Ni–N/C_3_EtOH, and Ni–N/C_3_H₂O were offset by 400, 800, and 1200 cm³ g⁻¹, respectively, for clarity.

Table S1 Textural properties of SBA-15 and the Ni–N/C_3_*X* catalysts

Material	Mean pore diameter[a] (nm)	BET surface area[b] (m^2 g^{-1})	Total pore volume[c] (cm^3 g^{-1})
SBA-15	12.7	408	1.18
Ni–N/C_3_Dry	5.1	739	1.21
Ni–N/C_3_Acetone	5.1	719	1.13
Ni–N/C_3_EtOH	5.1	710	1.16
Ni–N/C_3_H$_2$O	5.1	730	1.10

[a] Determined at the maximum point in the pore size distribution curve. [b] Calculated in the relative pressure range of 0.05–0.2. [c] Calculated at the relative pressure of 0.98–0.99.

Table S2 ICP−OES and EA results of Ni–N/C_3_*X* catalysts in wt%

Material	Ni[a]	C[b]	H[b]	N[b]	O[b]
Ni–N/C_3_Dry	1.68	77.09	1.75	9.58	9.86
Ni–N/C_3_Acetone	1.62	76.83	2.03	9.15	9.64
Ni–N/C_3_EtOH	1.53	76.27	1.94	9.43	9.28
Ni–N/C_3_H_2O	1.73	75.81	1.88	10.39	9.54

[a] Determined by ICP-OES analysis. [b] Determined by EA.
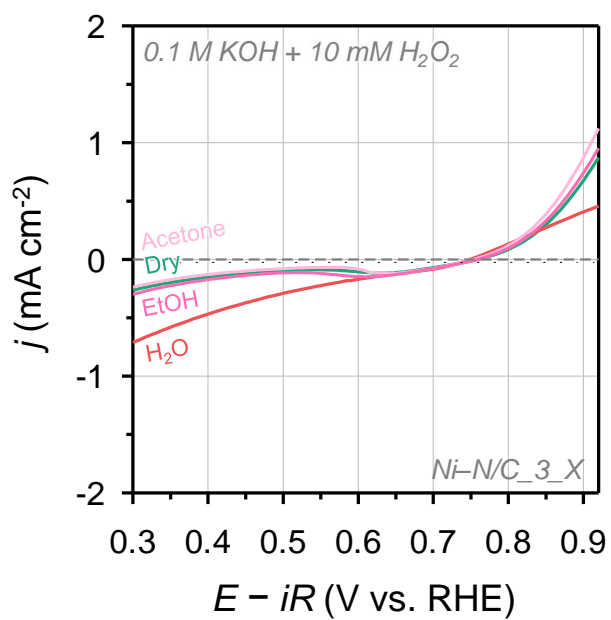
**Fig. S4** HPR polarization curves of Ni–N/C_3_*X* catalysts measured in N$_2$-saturated 0.1 M KOH containing 10 mM H$_2$O$_2$.
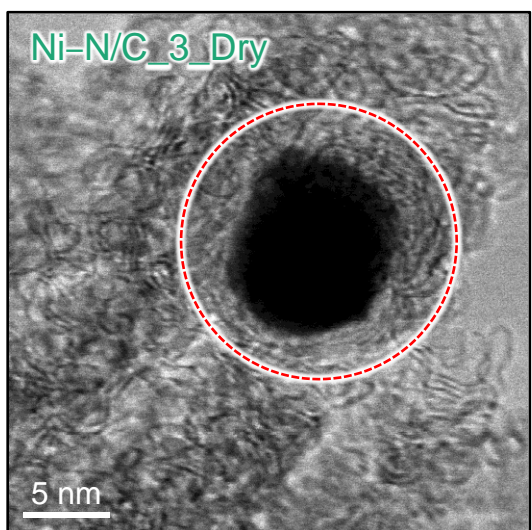
Fig. S5 High-magnification BR-STEM image of Ni–N/C_3_Dry catalyst.
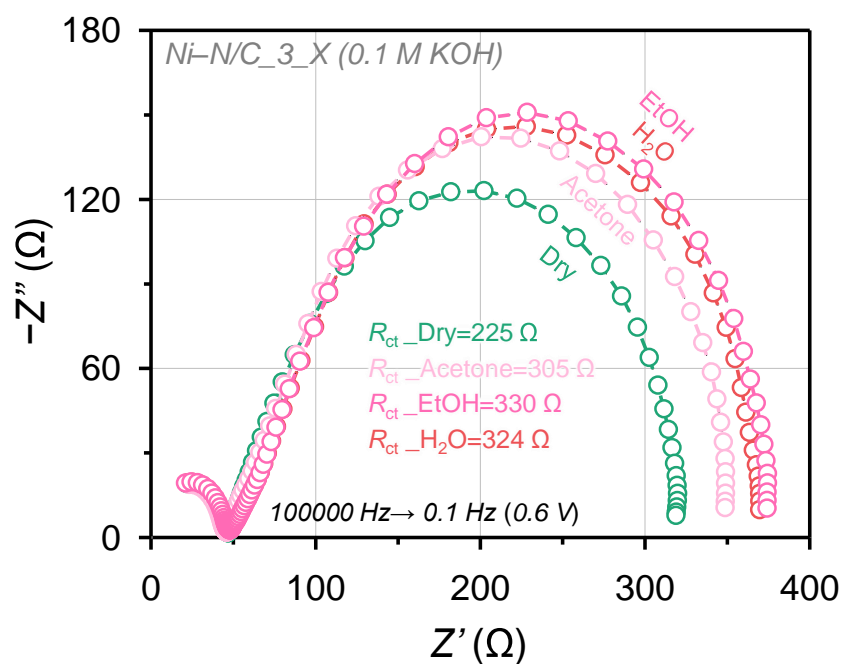
Fig. S6 Nyquist plots of Ni–N/C_3_X catalysts.
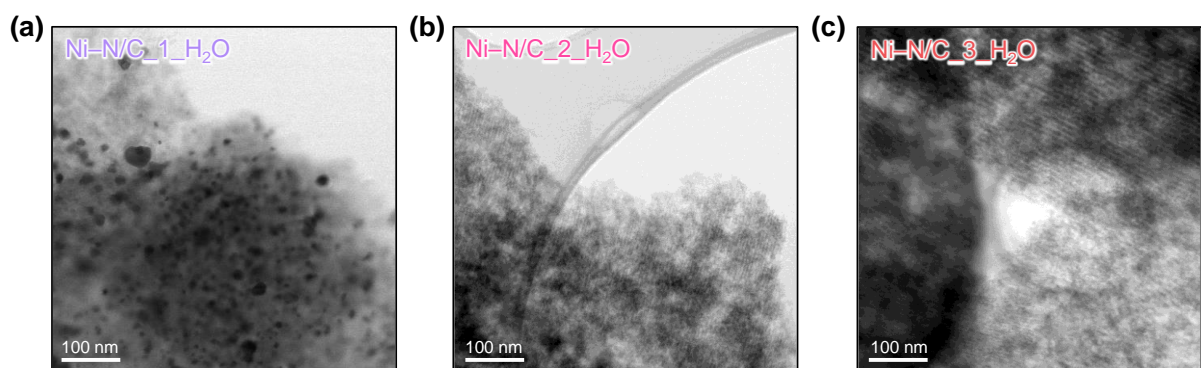
Fig. S7 BR-STEM images of (a) Ni–N/C_1_ H_2O, (b) Ni–N/C_2_ H_2O, and (c) Ni–N/C_3_ H_2O catalysts.
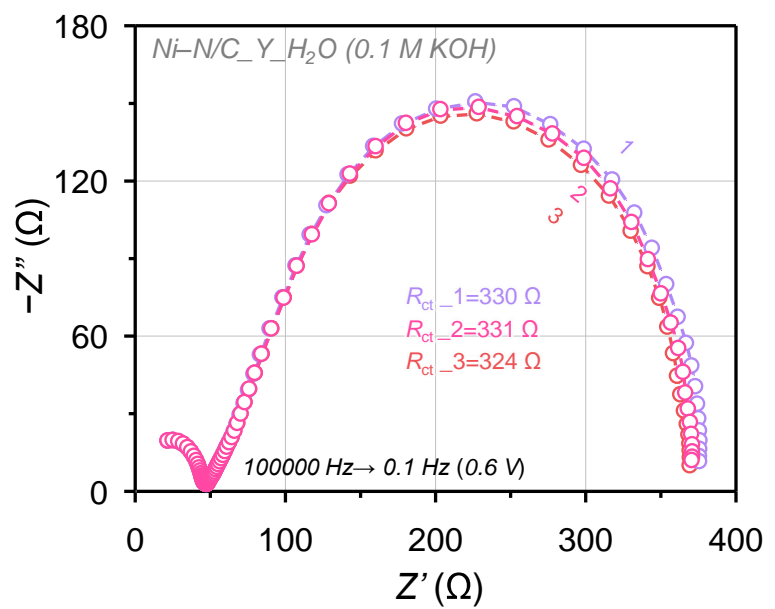
Fig. S8 Nyquist plots of Ni–N/C_*Y*_H₂O catalysts.
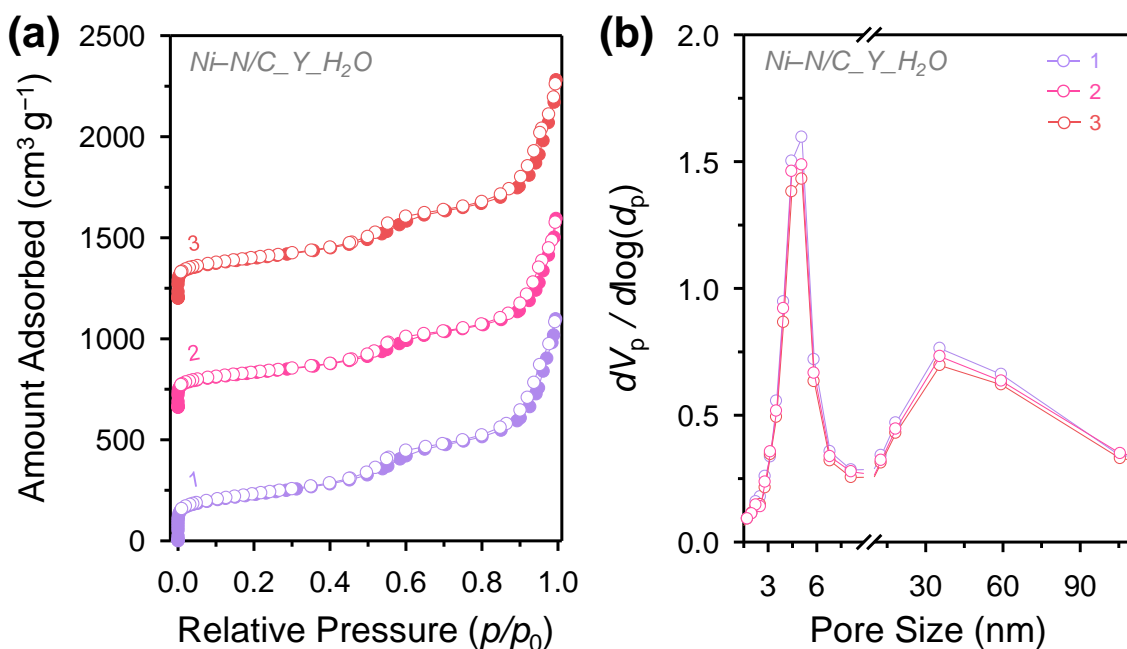
Fig. S9 (a) N$_2$ adsorption-desorption isotherms and (b) BJH pore size distribution curves obtained from the adsorption branch of the corresponding isotherms of Ni–N/C_*Y*_H$_2$O catalysts. The isotherms of Ni–N/C_2_H$_2$O and Ni–N/C_3_H$_2$O were offset by 600 and 1200 cm^3 g^{-1}, respectively, for clarity.

Table S3 Textural properties of SBA-15 and Ni–N/C_Y_H$_2$O catalysts

Material	Mean pore diameter[a] (nm)	BET surface area[b] (m^2 g^{-1})	Total pore volume[c] (cm^3 g^{-1})
SBA-15	12.7	408	1.18
Ni–N/C_1_H$_2$O	5.1	741	1.17
Ni–N/C_2_H$_2$O	5.1	773	1.11
Ni–N/C_3_H$_2$O	5.1	730	1.10

[a] Determined at the maximum point in the pore size distribution curve. [b] Calculated in the relative pressure range of 0.05–0.2. [c] Calculated at the relative pressure of 0.98–0.99.

Table S4 ICP-OES and EA results of Ni–N/C_Y_H$_2$O catalysts in wt%

Material	Ni[a]	C[b]	H[b]	N[b]	O[b]
Ni–N/C_1_H$_2$O	1.68	76.68	2.07	8.13	10.08
Ni–N/C_2_H$_2$O	1.53	76.95	1.93	8.77	9.42
Ni–N/C_3_H$_2$O	1.73	75.81	1.88	10.39	9.54

[a] Determined by ICP-OES analysis. [b] Determined by EA.
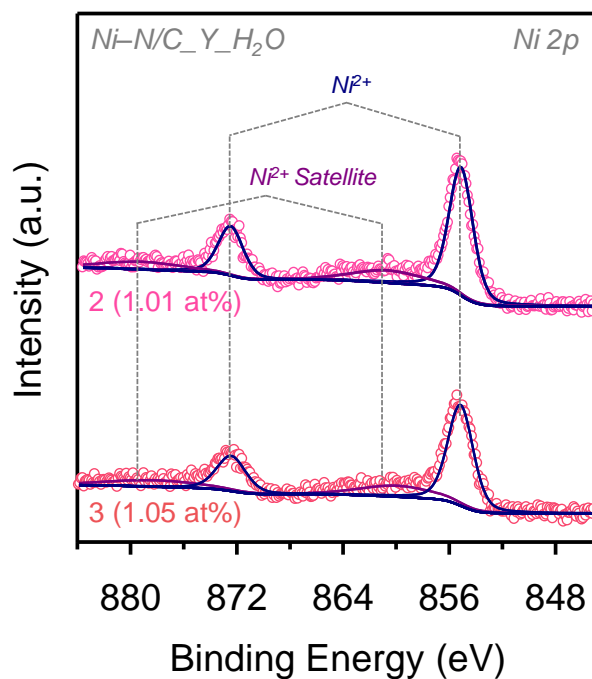
**Fig. S10** Ni 2p XPS spectra of Ni–N/C_2_H_2O and Ni–N/C_3_H_2O catalysts.
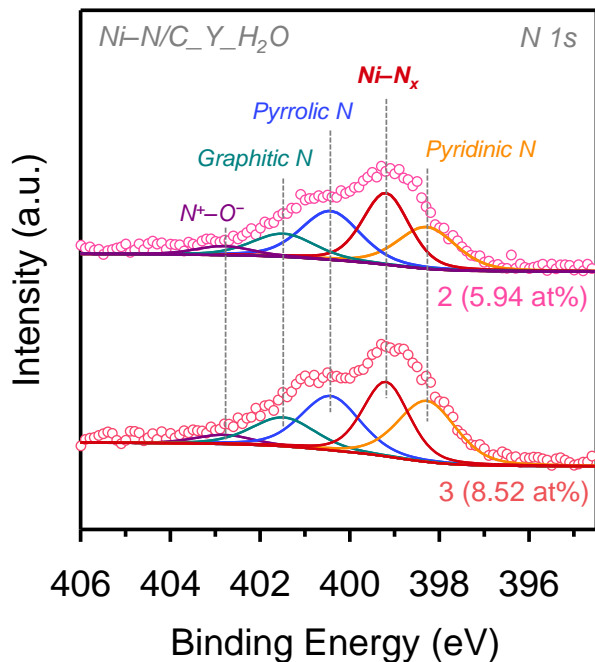
Fig. S11 N 1s XPS spectra of Ni–N/C_2_H₂O and Ni–N/C_3_H₂O catalysts.
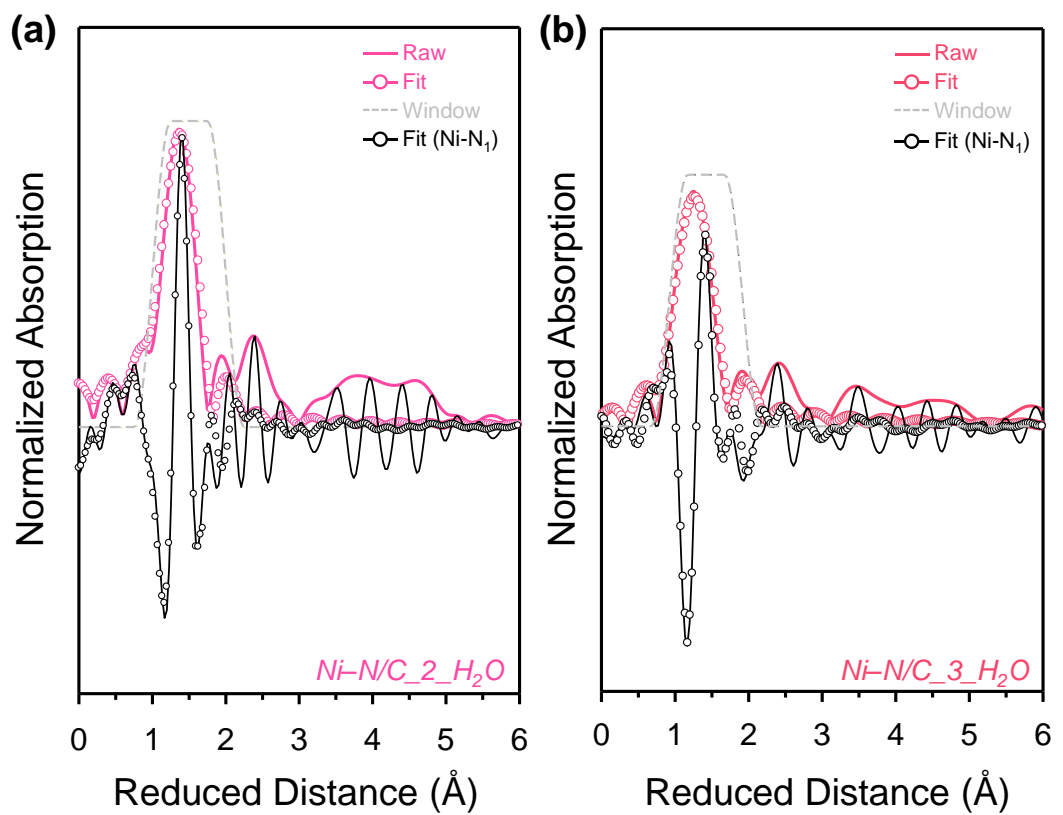
Fig. S12 EXAFS fitting spectra of the (a) Ni–N/C_2_H$_2$O and (b) Ni–N/C_3_H$_2$O catalysts in *R* space.
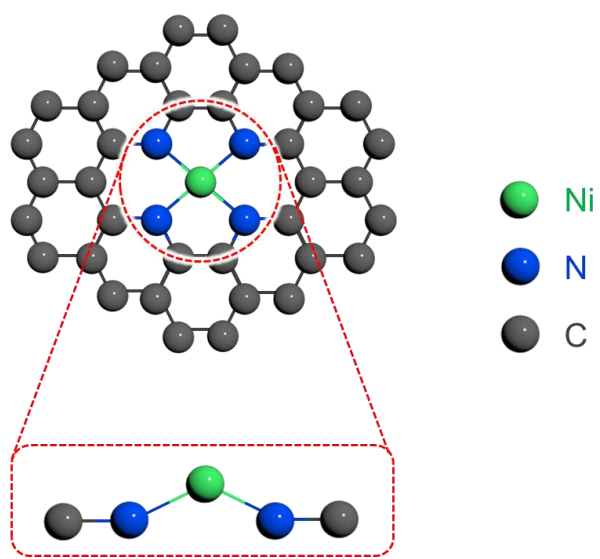
Fig. S13 Model structure for EXAFS fitting of the Ni–N/C_2_H$_2$O and Ni–N/C_3_H$_2$O catalysts.

Table S5 Summary of EXAFS fitting parameters for Ni–N/C_2_H_2O, Ni–N/C_3_H_2O, and Ni foil

Material	k range (Å^{-1})	R range (Å)	Scattering	CN[a]	R^{b} (Å)	$\sigma^{2\,c}$ (10^{-3}Å^{-2})	ΔE_0 (eV)	R factor (%)
Ni–N/C_2_H_2O	2.5–11.7	1.0–2.0	Ni–N$_1$	4.1 ± 0.3	1.88 ± 0.02	8.3 ± 3.6	4.5 ± 2.7	1.6
Ni–N/C_3_H_2O	2.5–11.7	1.0–2.0	Ni–N$_1$	3.9 ± 0.2	1.82 ± 0.04	7.7 ± 2.5	7.9 ± 1.1	0.9
Ni Foil	2.5–12.5	1.7–4.25	Ni–Ni$_1$	12	2.492 ±0.01	8.2 ± 1.5	5.9 ± 1.1	1.1
			Ni–Ni$_2$	6	3.524 ±0.01			
			Ni–Ni$_3$	24	4.317 ±0.01			
			Ni–Ni$_1$–Ni$_1$	48	3.739 ± 0.01			
			Ni–Ni$_1$–Ni$_2$	48	4.255 ± 0.01			

[a]Coordination number. [b]Interatomic distance. [c]Debye–Waller factor. [d]All Ni foil CN values were fixed to a theoretical values for *fcc* Ni to obtain the passive electron reduction factor (S_0^2) which was determined to be 0.87.
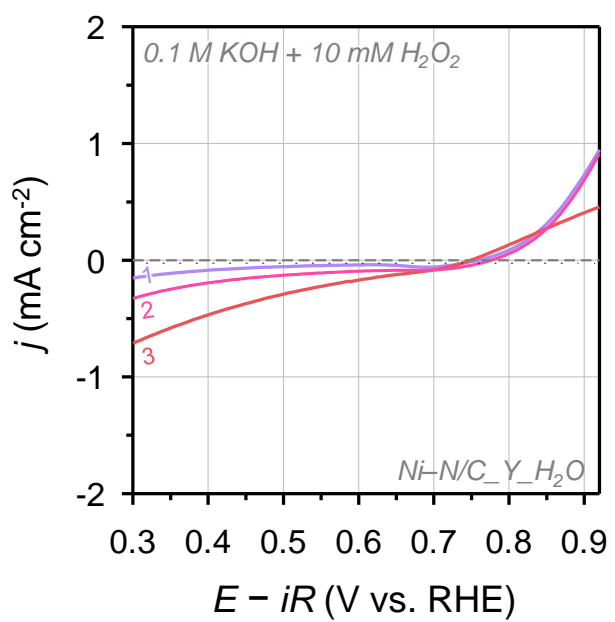
**Fig. S14** HPR polarization curves of Ni–N/C_*Y*_H₂O catalysts measured in N₂-saturated 0.1 M KOH containing 10 mM H₂O₂.

Table S6 Benchmarking electrochemical H_2O_2 production performance of Ni–N/C_3_H_2O catalyst with those of previously reported nonprecious metal ADCs and carbon-based catalysts in terms of mass activity and maximum H_2O_2 selectivity in 0.1 M KOH (or NaOH)

| Sample	Mass activity @ 0.70 V (A g^{-1})	Max. H_2O_2 selectivity by RRDE (%)	References
Ni–N/C_3_H_2O	**490.9**	**92**	**This work**
Co-N/C	35.7	65	S1
Fe-CNT	25.1	95	S2
Co$_1$-NG(O)	392.9	80	S3
Ni SA/G-O	9.9	94	S4
O-C (Al)	270.4	95	S5
Mo$_1$/OSG-H	34.0	95	S6
meso-Ni–N/C	61.4	82	S7
F-mrGO(600)	110.8	100	S8
O-CNT	29.9	90	S9
BN-C1	8.9	90	S10
NCMK3IL	19.1	86	S11
MesoC	1.3	80	S12
o-GOMC-1	73.1	93	S13
Oxo-G/$NH_3 \cdot H_2O$	1.9	82	S14
N-MFLG-8	3.0	95	S15
GNP$_{C=O,1}$	38.9	98	S16
NF-Cs	24.0	82	S17
OCB-120+CTAB	30.2	92	S18
OCNS$_{900}$	191.0	90	S19
HCB+0.5 KCl	201.3	87	S20
O-GOMC-5.5	120.6	92	S21
B-C	32.3	90	S22
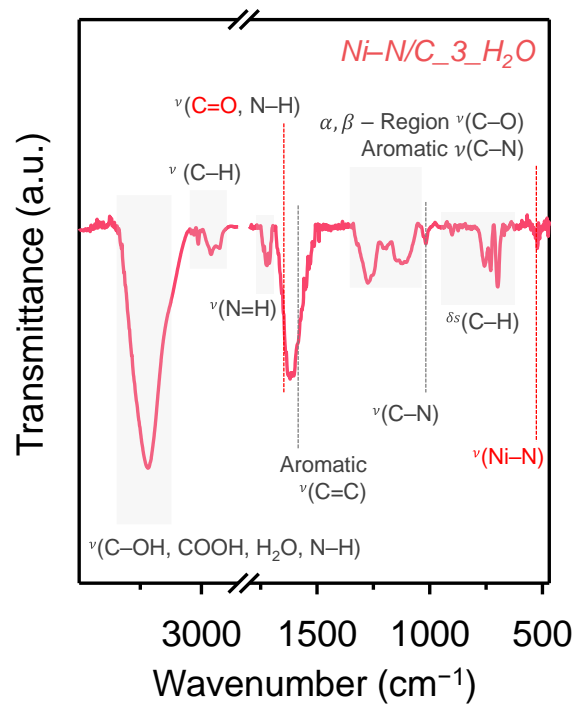
Fig. S15 FT-IR spectrum of Ni–N/C_3_H₂O catalyst.
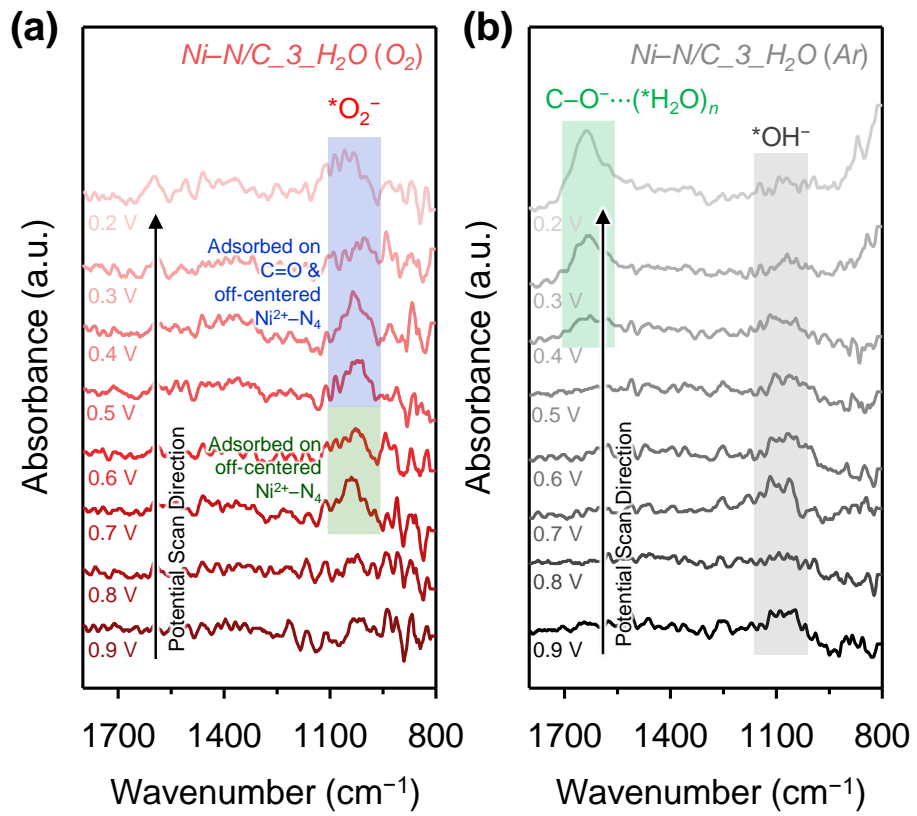
Fig. S16 In-situ ATR-SEIRAS spectra of Ni–N/C_3_H₂O catalyst collected in the (a) O₂-saturated and (b) Ar-saturated 0.1 M KOH electrolyte with 0.1 V intervals from 0.9 V to 0.2 V. The * symbol denotes catalyst surface.
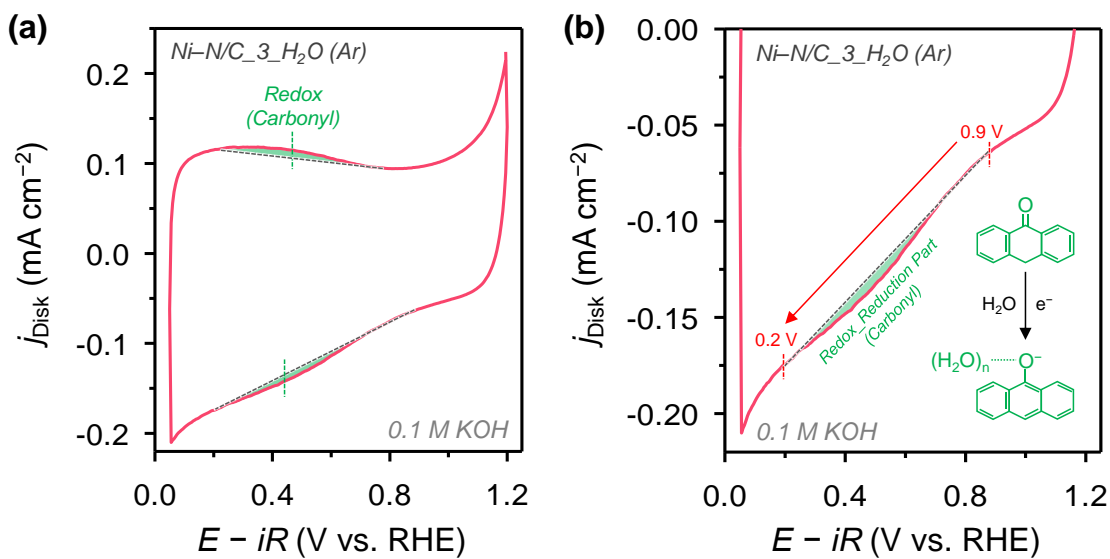
Fig. S17 (a) Full and (b) carbonyl reduction part enlarged CV curves of Ni–N/C_3_H$_2$O catalyst collected in Ar-saturated 0.1 M KOH at a scan rate of 20 mV s^{-1}.
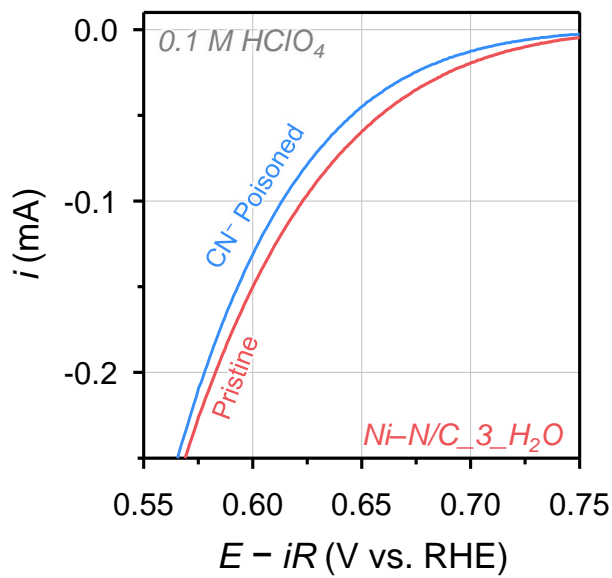
Fig. S18 ORR polarization curves of Ni–N/C_3_H₂O catalyst before and after CN⁻ poisoning.
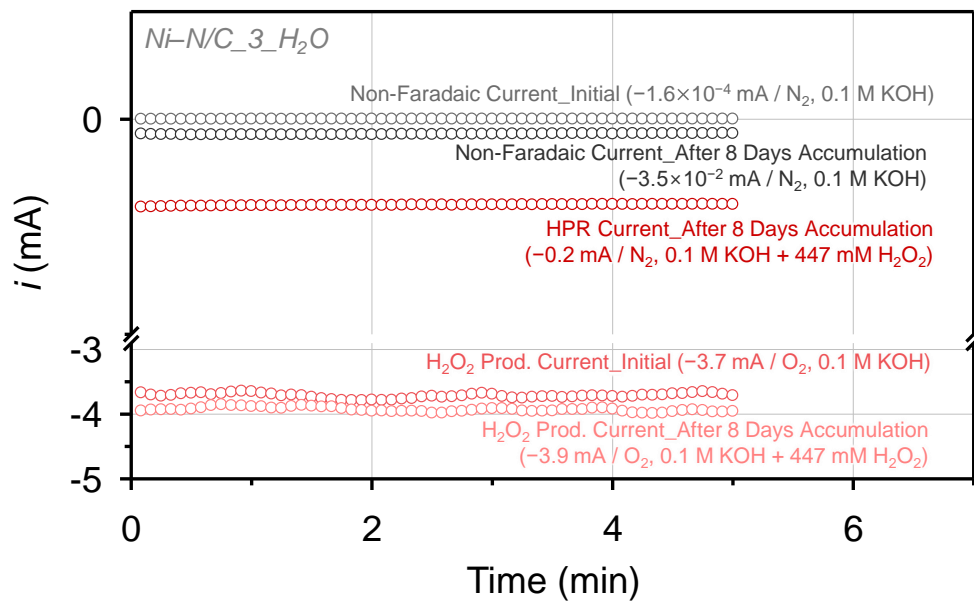
Fig. S19 The non-faradaic current, HPR current, and H_2O_2 production current responses of the eight-day-tested Ni–N/C_3_H$_2$O-coated electrode at 0.6 V (vs. RHE). The non-faradaic current and H_2O_2 production current responses of the fresh Ni–N/C_3_H$_2$O-coated electrode at 0.6 V (vs. RHE) were used as references.
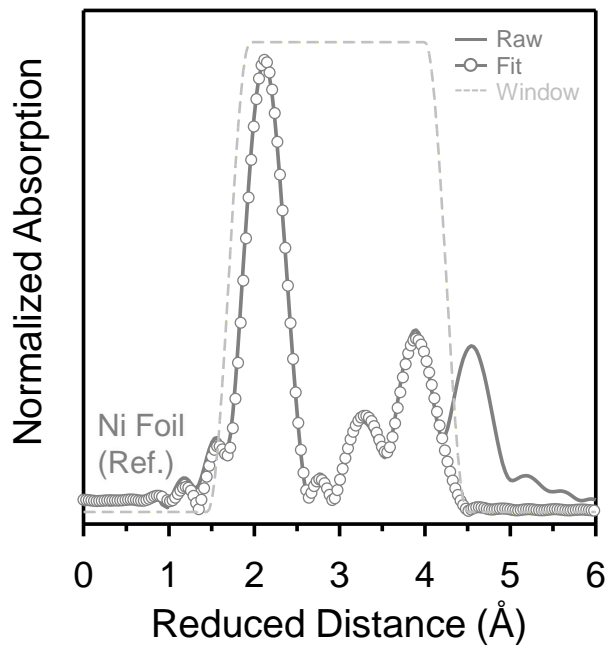
Fig. S20 EXAFS fitting spectra of Ni foil in the *R* space.
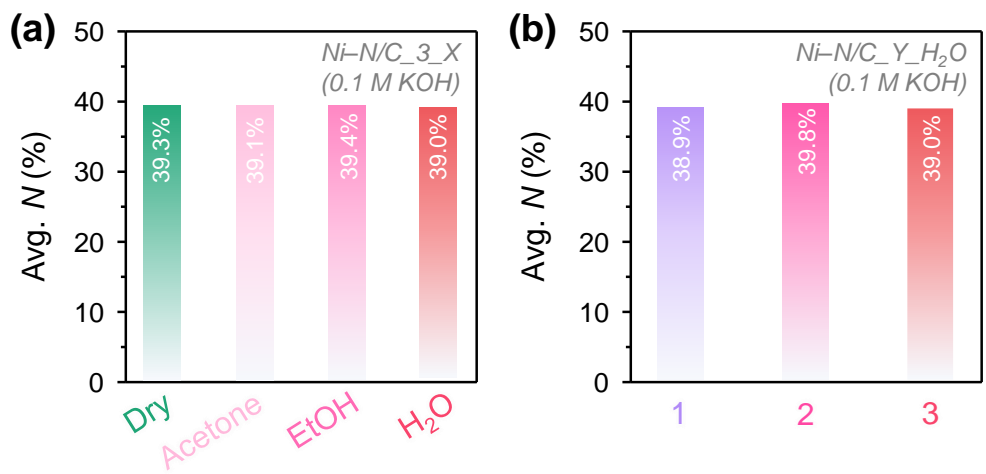
Fig. S21 Collection efficiency of (a) Ni–N/C_3_*X* and (b) Ni–N/C_*Y*_H$_2$O catalysts in 0.1 M KOH.

2. References

S1   Y. Sun, I. L. Silvioli, N. R. Sahraie, W. Ju, J. Li, A. Zitolo, S. Li, A. Bagger, L. Arnarson, X. Wang, T. Moeller, D. Bernsmeier, J. Rossmeisl, F. Jaouen and P. Strasser, *J. Am. Chem. Soc.*, 2019, **141**, 12372–12381.

S2   K. Jiang, S. Baek, A. J. Akey, C. Xia, Y. Hu, W. Liang, D. Schaak, E. Stabitski, J. K. Nørskov, S. Siahrostami and H. Wang, *Nat. Commun.*, 2019, **10**, 3997.

S3   E. Jung, H. Shin, B.-H. Lee, V. Efremov, S. Lee, H. S. Lee, J. Kim, W. H. Antink, S. Park, K.-S. Lee, S.-P. Cho, J. S. Yoo, Y.-E. Sung and T. Hyeon, *Nat. Mater.*, 2020, **19**, 436–442.

S4   X. Song, N. Li, H. Zhang, L. Wang, Y. Yan, H. Wang, L. Wang and Z. Bian, *ACS Appl. Mater. Interfaces.*, 2020, **12**, 17519–17527.

S5   Q. Yang, W. Xu, S. Gong, G. Zheng, Z. Tian, Y. Wen, L. Peng, L. Zhang, Z. Lu and L. Chen, *Nat. Commun.*, 2020, **11**, 5478.

S6   C. Tang, Y. Jiao, B. Shi, J.-N. Liu, Z. Xie, X. Chen, Q. Zhang and S.-Z. Qiao, *Angew. Chem., Int. Ed.*, 2020, **59**, 9171–9176.

S7   J. S. Lim, J. Kim, K.-S. Lee, Y. J. Sa, S. H. Joo, *Electrochim. Acta*, 2023, **444**, 142031.

S8   H. W. Kim, M. B. Ross, N. Kornienko, L. Zhang, J. Guo, P. Yang and B. D. McCloskey, *Nat. Catal.*, 2018, **1**, 282–290.

S9   Lu, Z., G. Chen, S. Siahrostami, Z. Chen, K. Liu, L. Liao, T. Wu, D. Lin, Y. Liu, T. F. Jaramillo, J. K. Nørskov and Y. Cui, *Nat. Catal.*, 2018, **1**, 156–162.

S10 S. Chen. Z. Chen, S. Siahrostami, D. Higgins, D. Nordlund, D. Sokaras, T. R. Kim, Y. Liu, X. Yan, E. Nilsson, R. Sinclair, J. K. Nørskov, T. F. Jaramillo and Z. Bao, *J. Am. Chem. Soc.*, 2018, **140**, 7851–7859.

S11 Y. Sun, I. Sinev, W. Ju, A. Bergmann, S. Dresp, S. Kuhl, C. Spöri, H. Schmies, H. Wang, D. Bernsmeier, B. Paul, R. Schmack, R. Kaehnert, B. Roldan Cuenya and P. Strasser, *ACS Catal.*, 2018, **8**, 2844–2856.

S12 S. Chen. Z. Chen, S. Siahrostami, T. R. Kim, D. Nordlund, D. Sokaras, S. Nowak, J. W. F. To, R. Sinclair, J. K. Nørskov, T. F. Jaramillo and Z. Bao, *ACS Sustainable Chem. Eng.*, 2018, **6**, 311–317.

S13 Y. J. Sa, J. H. Kim and S. H. Joo, *Angew. Chem., Int. Ed.*, 2019, **58**, 1100–1105.

S14 L. Han, Y. Sun., S. Li, C. Cheng, C. E. Halbig, P. Feicht, J. L. Hübner, P. Strasser and S. Eigler, *ACS Catal.*, 2019, **9**, 1283–1288.

S15 L. Li, C. Tang, Y. Zheng, B. Xia, X. Zhou, H. Xu and S.-Z. Qiao, *Adv. Energy Mater.*, 2020, **10**, 2000789.

S16 G.-F. Han, F. Li, W. Zou, M. Karamad, J.-P. Jeon, S.-W. Kim, S.-J. Kim, Y. Bu, Z. Fu, Y. Liu, S. Siahrostami and J.-B. Baek, *Nat. Commun.*, 2020, **11**, 2209.

S17 W. Wang, X. Lu, P. Su, Y. Li, J. Cai, Q. Zhang, M. Zhou and O. Arotiba, *Chemosphere*, 2020, **259**, 127423.

S18 K.-H. Wu, D. Wang, X. Lu, X. Zhang, Z. Xie, Y. Liu, B.-J. Su, J.-M. Chen, D.-S. Su, W. Qi and S. Guo, *Chem*, 2020, **6**, 1443–1458.

S19   S. Chen, T. Luo, K. Chen, Y. Lin, J. Fu, K. Liu, C. Cai, Q. Wang, H. Li, X. Li, J. Hu, H. Li, M. Zhu and M. Li, *Angew. Chem., Int. Ed.*, 2021, **60**, 16607–16614.

S20   J. Lee, J. S. Lim, G. Yim, H. Jang, S. H. Joo and Y. J. Sa, *ACS Appl. Mater. Interfaces.*, 2021, **13**, 59904–59914.

S21   J. S. Lim, J. H. Kim, D. S. Baek, K. Ihm, T. J. Shin, Y. J. Sa and S. H. Joo, *Chem*, 2021, **19**, 436–442.

S22   Y. Xia, X. Zhao, C. Xia, Z.-Y. Wu, P. Zhu, J. Y. Kim, X. Bai, G. Gao, Y. Hu, J. Zhong, Y. Liu and H. Wang, *Nat. Commun.*, 2021, **12**, 4225.